MAX-PLANCK-INSTITUT FÜR PLASMAPHYSIK

GARCHING BEI MÜNCHEN

THREE-DRIFT-WAVE INTERACTION AT FINITE PARALLEL WAVELENGTH: BIFURCATIONS AND TRANSITION TO TURBULENCE

Dieter Biskamp and He Kaifen*)

IPP 6/241 August 1984

*)
Present address: Institute of Low Energy Nuclear Physics,
Beijing Normal University, Beijing, China

Die nachstehende Arbeit wurde im Rahmen des Vertrages zwischen dem Max-Planck-Institut für Plasmaphysik und der Europäischen Atomgemeinschaft über die Zusammenarbeit auf dem Gebiete der Plasmaphysik durchgeführt.

Abstract:

The generic properties of the nonlinear interaction of three driftwaves with finite $k_{\parallel}$ are investigated. The different types of stationary or quasi-stationary states are characterized by the bifurcation diagram in γ_1, κ parameter space, where γ_1 measures the mode excitation and κ the parallel wave number. The transition to turbulence corresponds exactly to the Ruelle-Takens picture: steady state → periodic solution → doubly periodic solution → turbulence, in contrast to the period-doubling route usually observed in low-dimensional dynamic systems.

I. INTRODUCTION

Drift-wave turbulence seems to be the dominant micro-fluctuation process in tokamak plasmas and is the most likely cause of the anomalous transport observed. Several recent experimental studies[1)2)] have shown the presence of small-scale turbulent density fluctuations with typically $k_\perp \rho_i \sim 1$, where ρ_i is the ion gyroradius, which appear to exist across the whole plasma cross-section. Although average amplitudes may differ significantly, being $\tilde{n}/n_o \sim 10^{-2} - 10^{-3}$ in the plasma interior and more like $\tilde{n}/n_o \sim 10^{-1}$ at the plasma edge[2)], all these density fluctuations are generally associated with nonlinear drift waves. Wave number spectra are broad and so are the frequency spectra for fixed values of the wave number. The latter observation is of particular importance, indicating a state of strong turbulence which cannot be described by standard weak turbulence theory. Drift waves exist owing to the presence of a density or pressure gradient. They may be excited by various instability mechanisms, e.g. collisions (dissipative drift instability), inverse electron Landau damping (universal instability) or trapped particles (trapped electron instability). While the classification of linear drift instabilities is rather complete, nonlinear theories describing the saturated and probably turbulent state are still quite crude, emphasizing various nonlinear saturation effects. One may generally distinguish between two approaches: a) The driving mechanism is turned off by a nonlinear process, e.g. by a modification of resonant particle orbits, which occurs at an amplitude sufficiently low to preserve the linear mode structure essentially. An example is the theory of stabilization of the universal instability due to resonant electron diffusion[3)]. However, since the frequency spectra would be rather narrow, it appears that this saturation effect is not the dominant one in typical tokamak plasmas. b) Amplitudes are excited to le-

vels sufficiently high for fluid-type nonlinearities to become important as in hydrodynamic turbulence. While the total wave energy still depends on the magnitude of the excitation, e.g. the linear instability growth rates, the spectra are essentially determined by the mode-coupling processes and have rather universal properties. Several different mode-coupling theories of drift-wave turbulence have been discussed in recent years[4)5)], each emphasizing the importance of a particular nonlinear term in the fluid equations.

Because of the quadratic form of the nonlinear terms the basic interaction involves a triple of modes with $\Sigma \underset{\sim}{k}_i = 0$. Hence the lowest-order model contains just three modes. Though such radically truncated systems cannot of course yield a quantitative description of the turbulence, it is quite generally assumed that they already contain essential features thereof. They may give rise to, for instance, random or chaotic behaviour, the best known and most intensively studied example being the Lorenz equations[6)] as the simplest model of Rayleigh-Bénard convection. For the drift-wave problem a three-wave model was recently investigated by Terry and Horton[7)]. Although these authors find stationary turbulent states to exist under certain conditions, the average wave amplitudes are too high relative to the usual estimates. In a subsequent article[8)] the authors were then able to show that including substantially more modes (~ 20) considerably reduced the turbulence levels. Using a model with even more modes (~ 400) Waltz[9)] obtained turbulence amplitudes in rough agreement with experimental observations on tokamaks.

In the present paper we return to the three-wave approximation but refine the physics included. It is well known that drift waves are strongly influenced by the shear of the magnetic field. In the presence of shear they generally have a finite parallel component of the wave number and thus couple to sound waves. This coupling gives rise to two different effects. Since sound waves

propagate along the magnetic field, they are easily dissipated by collisional viscosity or Landau damping and thus lead to effective damping of the coupled wave system, which one could call a sound-drift-wave. On the other hand, the coupling changes the dispersion properties and introduces a new nonlinear term, leading to lower effective turbulence levels even without the additional parallel dissipation. It is this second effect which we include in our model by allowing finite $k_{\parallel}$.

In a preceding paper[10] we restricted our attention to drift waves excited by electron-wave resonance as discussed by Terry and Horton[7]. Our main result was that for $k_{\parallel} \sim 0(1)$ (in the units to be given in Sec. II) the saturation turbulence levels are substantially smaller than for $k_{\parallel} = 0$ and are consistent with conventional estimates. Here we now investigate the generic properties of the three-sound-drift-wave equations more closely. The model is of substantially higher dimensionality, having ten independent dynamic variables as compared with four in the Terry - Horton model, $k_{\parallel} = 0$. Our aim is to give a complete overview of the asymptotic (regular or turbulent) solutions as a function of two parameters κ and γ_1 characterizing the size of the parallel wave numbers and the mode excitation.

The organization of the paper is as follows: In Sec. II the model equations are derived and some of their basic properties are presented. These equations are solved numerically. The numerical approach and the different diagnostic methods of analyzing the long-time properties of the solutions are discussed in Sec. III. Section IV gives a general discussion of the bifurcation diagram, while in Sec. V several specific paths in γ_1, κ space are followed in greater detail. Section VI summarizes the results.

II. MODEL EQUATIONS

In the presence of magnetic shear there is in general a parallel (to the magnetic field) variation of the density fluctuation n' of a drift wave which generates a parallel ion flow J, where n and J satisfy the equations

$$\frac{\partial n'}{\partial t} + \nabla_{\parallel} J + \nabla_{\perp} \cdot \left[n (\underset{\sim}{v}_E + \underset{\sim}{v}_p) \right] = 0 \qquad (1)$$

$$\frac{\partial J}{\partial t} + \frac{1}{m} \nabla_{\parallel} P + \frac{ne}{m} \nabla_{\parallel} \phi + \underset{\sim}{v}_E \cdot \nabla_{\perp} J = 0 \qquad (2)$$

Here

$$\underset{\sim}{v}_E = - \frac{c}{B_o} \nabla_{\perp} \phi \times \hat{b}$$

$$\underset{\sim}{v}_p = - \frac{c}{\Omega_{ci} B_o} \left[\frac{\partial \nabla_{\perp} \phi}{\partial t} + (\underset{\sim}{v}_E \cdot \nabla_{\perp}) \nabla_{\perp} \phi \right]$$

are the $\underset{\sim}{E} \times \underset{\sim}{B}$ and polarization drifts, respectively, $n \equiv n_o + n'$, n_o is the unperturbed ion density, $\underset{\sim}{B}_o$ is the applied magnetic field, $\hat{b} = \underset{\sim}{B}_o / B_o$, P is the ion pressure, which will be neglected in the following, e and m are the ion charge and mass, Ω_{ci} is the ion gyro-frequency, and ϕ is the fluctuating electrostatic potential.

We use the following units: $(T_e/n_o e)(\rho_s/L_n)$ for ϕ, $n_o c_s \rho_s / L_n$ for J, L_n/c_s for t, and $1/L_n$ and $1/\rho_s$ for $\nabla_{\parallel}$ and $\nabla_{\perp}$ respectively. Here L_n is a length characterizing the average density gradient, c_s is the sound speed and $\rho_s = c_s/\Omega_{ci}$.

In the presence of shear the global configuration is necessarily inhomogeneous. In slab geometry one usually chooses

coordinates such that $\underset{\sim}{B} = B_o(\hat{z} + \frac{x}{L_s}\hat{y})$, where L_s is called the shear length. To define individual Fourier modes and their interaction, one must consider local (in x) Fourier transforms ϕ_k, which is only possible if $k_x\rho_s >> L_n/L_s$, so that modes may phase-mix and become statistically independent over a distance where the direction of $\underset{\sim}{B}$ and hence the parallel components of the wave numbers do not vary substantially. This picture of "radially" local modes is just opposite to that of global eigenmodes which are strongly correlated in x. However, as has recently been shown[11], the latter do not persist at finite amplitude, but one has instead $k_x \sim k_y$. Since typically $k_y\rho_s \sim 1$ and $L_s/L_n \sim 20$, the above condition for the validity of the local Fourier representation is satisfied.

If the response of the electrons is assumed to be linear, then by using the quasi-neutrality condition the Fourier component of the density fluctuation n_k' is related to that of the fluctuating potential ϕ_k by the following expression:

$$n_k' = \phi_k (1 - i\delta_k) \quad ,$$

where δ_k results from the nonadiabatic response of the electrons.

Since the mechanisms for the nonlinear interaction coming from the terms $\nabla \cdot n (\underset{\sim}{v}_E + \underset{\sim}{v}_p)$ have already been studied, we should like to shed some light on the effect of the third nonlinear term, $\underset{\sim}{v}_E \cdot \nabla J$. We therefore omit for the moment the nonlinear terms in eq. (1). In this case, eqs. (1) and (2) reduce to (writing $i\delta_k \, \partial\phi_k/\partial t = \gamma_k \phi_k$)

$$\frac{d\phi_k}{dt} = \gamma_k\phi_k - i\, k_y\phi_k - i\, k_{\parallel}J_k \quad , \tag{3}$$

$$\frac{dJ_k}{dt} = - i k_{\shortparallel} \phi_k + \sum_{\substack{k' + k'' = k \\ \sim \quad \sim \quad \sim}} (\underset{\sim}{k}'_{\perp} \times \underset{\sim}{k}''_{\perp}) \cdot \hat{b} \; \phi_{k'} \, J_{k''} \; . \qquad (4)$$

The linear dispersion relation derived from eqs. (3) and (4) is

$$\omega^2 - (k_y + i \gamma) \omega - K^2 = 0 \; , \qquad (5)$$

K being written instead of $k_{\shortparallel}$ for the sake of simpler notation. For $K << k_y$ and $\gamma << \omega$, the solution of (5) is

$$\omega_k = k_y \left(1 + \frac{K^2}{k_y^2}\right) . \qquad (6)$$

We now investigate the simplest case of just three interacting modes which form a triangle with $\underset{\sim}{k}_1 + \underset{\sim}{k}_2 + \underset{\sim}{k}_3 = 0$. Their projected components on the magnetic line $\underset{\sim}{B}$ are K_1, K_2, K_3 , respectively. We express the j-th mode ϕ_j in terms of real positive amplitude a_j and real phase angle α_j:

$$\phi_j (t) = a_j (t) \exp \{- i \alpha_j (t)\} \; . \qquad (7)$$

$\alpha_j(t)$ can be divided into two parts, $\alpha_j(t) = \omega_j t - \tilde{\alpha}_j(t)$, on the assumption that $\tilde{\alpha}_j(t) << \omega_j$, where ω_j is given by eq. (6). If weak nonlinearity is assumed, eq. (4) for the j-th mode can be written

$$\frac{dJ_j}{dt} = - iK_j \phi_j - A \left(\frac{K_\ell}{\omega_\ell} - \frac{K_m}{\omega_m}\right) \phi_\ell^* \, \phi_m^* \; , \qquad (8)$$

where ϕ_j^* is the complex conjugate of ϕ_j, $A = \frac{1}{2} \hat{b} \cdot \underset{\sim}{k}_1 \times \underset{\sim}{k}_2$

and $\{j, \ell, m\}$ is a cyclic permutation of $\{1, 2, 3\}$. Here we have neglected higher orders in the nonlinear terms.

Substituting eq. (7) in the time derivative of eq. (3), using relations (6) and (8) and neglecting small terms, we obtain the model equations for the amplitudes a_j and total phase $\alpha = \alpha_1 + \alpha_2 + \alpha_3$:

$$\frac{da_j}{dt} = \Gamma_j a_j - A D_j a_\ell a_m \cos\alpha , \tag{9}$$

$$\frac{d\alpha}{dt} = \Delta\omega + A \sum_{\{j,\ell,m\}} D_j \frac{a_\ell a_m}{a_j} \sin\alpha , \tag{10}$$

where $\Gamma_j = \gamma_j/(1 + K_j^2/\omega_j^2)$, $D_j = \frac{K_j}{\omega_j}(\frac{K_\ell}{\omega_\ell} - \frac{K_m}{\omega_m})/(1 + \frac{K_j^2}{\omega_j^2})$ and $\Delta\omega = \omega_1 + \omega_2 + \omega_3$. Equations (9) and (10) have the same form as discussed by Terry and Horton[7] for real susceptibilities. In keeping with their derivation the conditions for steady state are

$$\text{sgn}\,(\gamma_j) = -\,\text{sgn}\,(\gamma_\ell) = -\,\text{sgn}\,(\gamma_m), \tag{11}$$

$$\text{sgn}\,(D_j) = -\,\text{sgn}\,(D_\ell) = -\,\text{sgn}\,(D_m). \tag{12}$$

On the assumption that $\gamma_j > 0$, γ_ℓ, $\gamma_m < 0$, these conditions are satisfied only if the mode j has a parallel phase velocity intermediate to those of the other two modes,

$$\frac{\omega_m}{K_m} < \frac{\omega_j}{K_j} < \frac{\omega_\ell}{K_\ell} \tag{13}$$

(or the inverse inequality). This is also the condition for parametric decay of a large amplitude wave j into two waves, one with higher phase velocity, the other with lower. We thus find that

the nonlinear term in eq. (2) has a stabilizing effect in the three-sound-drift-wave interaction when the inequality (13) is satisfied.

Let us now turn to the full nonlinear equations (1), (2). Writing in addition to eq. (7)

$$J_j(t) = b_j(t) \exp\{-i\beta_j(t)\},$$

we derive the three-mode truncation model in terms of the ten real dynamic variables a_j, b_j, $\theta_j \equiv \alpha_j - \beta_j$, and $\alpha \equiv \alpha_1 + \alpha_2 + \alpha_3$:

$$\frac{da_j}{dt} = \gamma_j a_j + K_j b_j \sin\theta_j - A(F_j\cos\alpha - G_j\sin\alpha)\, a_\ell\, a_m\,, \tag{14}$$

$$\frac{db_j}{dt} = -K_j\, a_j \sin\theta_j + 2A\left[a_\ell b_m \cos(\alpha-\theta_m-\theta_j) - a_m b_\ell \cos(\alpha-\theta_j-\theta_\ell)\right], \tag{15}$$

$$\frac{d\theta_j}{dt} = \omega_j + K_j\left(\frac{b_j}{a_j} - \frac{a_j}{b_j}\right)\cos\theta_j + A(F_j\sin\alpha + G_j\cos\alpha)\,\frac{a_\ell a_m}{a_j} + 2A\left[a_\ell b_m \sin(\alpha-\theta_m-\theta_j) - a_m b_\ell \sin(\alpha-\theta_j-\theta_\ell)\right]/b_j, \tag{16}$$

$$\frac{d\alpha}{dt} = \Delta\omega + \sum_{j=1}^{3} \frac{K_j b_j}{a_j}\cos\theta_j + A \sum_{\{j,\ell,m\}} (F_j\sin\alpha + G_j\cos\alpha)\frac{a_\ell a_m}{a_j}. \tag{17}$$

Here F_j, G_j are the coupling coefficients arising from the nonlinear polarization drift and the $\underset{\sim}{E}\times\underset{\sim}{B}$ density convection, respectively, $F_j = k_{\perp\ell}^2 - k_{\perp m}^2$ and $G_j = \delta_{k_\ell} - \delta_{k_m}$, as given in Ref. 7. The energy balance can easily be obtained from eqs. (14) and (15)

$$\frac{dW}{dt} \equiv \frac{d}{dt}\,\frac{1}{2}\sum_{j=1}^{3}(a_j^2 + b_j^2) = \sum_{j=1}^{3} \gamma_j a_j^2\,. \tag{18}$$

Using an appropriate volume element in the ten-dimensional phase-space (generalized cylindrical coordinates to account for the positivity of the amplitude factors a_j , b_j),

$$dV = \prod_{j=1}^{3} \{da_j^2 \, d\, b_j^2 \, d\, \theta_j\} \, d\, \alpha \, , \tag{19}$$

one can easily calculate the change of dV from eqs. (14) - (17):

$$\frac{dV}{dt} = \sum_{j=1}^{3} \{\frac{1}{a_j} \frac{\partial}{\partial a_j} a_j \frac{da_j}{dt} + \frac{1}{b_j} \frac{\partial}{\partial b_j} b_j \frac{db_j}{dt} + \frac{\partial}{\partial \theta_j} \frac{d\theta_j}{dt}\} + \frac{\partial}{\partial \alpha} \frac{d\alpha}{dt}$$

$$= \sum_{j=1}^{3} 2 \gamma_j \, . \tag{20}$$

We thus see that the volume changes uniformly over all phase space. A necessary condition for bounded asymptotic solutions to exist is that $\gamma_t = \gamma_1 + \gamma_2 + \gamma_3 < 0$.

Equations (14) - (17) are a generalization of the three-wave equations discussed in Ref. 7, to which they reduce for $K_j = 0$. In a parallel paper we investigated the effect of K on the solution for values of parameters F_j, G_j, γ_j, ω_j corresponding to electron drift waves driven by a particular instability. In the present paper we choose the parameters somewhat more arbitrarily in order to study the generic properties of eqs. (14) - (17). While for realistic drift wave parameters solutions are mostly turbulent, we concentrate on cases where regular solutions, in particular steady states, also exist, so that the transition to turbulence determined by a particular sequence of bifurcations can be followed. As outlined in Ref. 7, stable steady-state solutions are most easily obtained if both F_j and G_j satisfy condition (12). In particular, we choose the values of F_j, G_j, γ_2, γ_3, and $\Delta\omega$ as in Fig. 5 of Ref. 7. The linear frequencies ω_j are chosen such that D_j also satisfy eq. (12), which

according to the discussion given above should further increase the probability of obtaining a steady-state solution. If a coordinate system is assumed such that $\underset{\sim}{k}_j \cdot \hat{z} = 0$, the parallel components K_j are given by the y-component of the magnetic field, $K_j/k_{yj} = \kappa = B_y/B_o$. Having thus fixed the parameters F_j, G_j, $\underset{\sim}{k}_j$, ω_j, γ_2, γ_3, $F_j = \{0.297, -0.237, -0.06\}$, $G_j = \{-0.2247, 0.2012, 0.0235\}$, $\underset{\sim}{k}_1 = (0.8935, 1.2048)$, $\underset{\sim}{k}_2 = (-0.4436, -0.8032)$, $\underset{\sim}{k}_3 = (-0.4499, -0.4016)$, $\omega_j = \{0.47065, -0.25615, -0.2945\}$, $\Delta\omega = 0.08$, $\gamma_2 = -0.25$, $\gamma_3 = -0.0191$, we study the properties of the time-asymptotic solutions as functions of the excitation strength γ_1, $0 < \gamma_1 < 0.2691$ (the upper boundary corresponding to $\gamma_t = 0$) and the parallel wave numbers, characterized by κ, $0 \leqq \kappa \lesssim 1$.

III. NUMERICAL SOLUTION AND DIAGNOSTICS

Except for very special cases, eqs. (14) - (17) can only be solved numerically. We first compute steady-state solutions. We solve the set of nonlinear equations resulting from setting the l.h.s. of (14) - (17) equal to zero, using a generalized Newton's method. To examine the stability of these solutions, we consider the corresponding linear eigenmode equations. A necessary and sufficient condition for stability is that all eigenvalues γ (with $d/dt = \gamma$) have negative real parts. In the case of instability the actual solution must be obtained from the time-dependent equations. These are solved by a standard Runge - Kutta IV method. As can be anticipated from eqs. (16) and (17), problems could arise if a_j or b_j come close to zero. Special care has to be taken in such an event. Starting from either the (unstable) steady state or from the solution in a neighboring point in γ_1, κ space, time integration was performed over a sufficiently long period to allow the solution to settle into the asymptotic (quasi-)stationary state.

Various types of numerical diagnostics are used to quantify

the properties of the asymptotic solutions: a) Time traces of a_j, b_j, $\cos\alpha$, $\cos\theta_1$. For regular (periodic or quasi-periodic) solutions these give a rather good indication whether or not the solution has become stationary. Strongly turbulent solutions are easily identified, but the transition from regular to turbulent behaviour is difficult to recognize. In certain cases solutions have been followed for up to 20,000 time units. b) Frequency spectra of a_1. As in experimental studies of Rayleigh-Bénard convection or similar systems, frequency spectra, if taken over sufficiently long times, seem to give the best characterization of a dynamic state. Simply or multiply periodic solutions are easily verified and well distinguished from a turbulent state. They are thus very sensitive diagnostic tools to study bifurcations, in particular the transition to turbulence. Frequency spectra are obtained by Fourier-analyzing time traces of $a_1(t)$ over typically 2000 to 4000 time units, using 16,000 to 32,000 grid points. c) Poincaré maps. Various types of Poincaré maps are considered. In most cases the hyperplane, whose intersections with the phase space orbit is recorded, are given by $\cos\alpha = 0$, either $\alpha = \frac{\pi}{2}$ mod 2π or $\alpha = \frac{3\pi}{2}$ mod 2π. Since only two-dimensional projections of the nine-dimensional hyperplane are practically useful, there are 36 different combinations of variables, only a few of which have actually been analyzed, mainly a_2, a_3 vs a_1, and b_2, b_3 vs b_1. While periodic orbits (limit cycles) and doubly periodic orbits (2 - tori) can thus be rather convincingly identified, it is difficult to distinguish in this manner between higher-dimensional solutions (e.g. 3 - tori) and truly chaotic solutions. d) one-dimensional maps, e.g. a_1^{n+1} vs. a_1^n. In contrast to strongly damped systems with a large phase space contraction rate such as the Lorenz model[6] or the three-wave system recently investigated by Wersinger et al.[12], the present equations do not lead to a quasi-one-dimensional map in the turbulent case. This type of map is therefore less useful here.
e) Maximum Liapunov exponent σ. This quantity characterizes the ex-

ponential divergence of neighbouring phase space orbits in the turbulent case. We use a definition introduced by Benettin et al.[13] which is particularly suitable when numerically integrating a system of differential equations such as eqs (14) - (17):

$$\sigma = \lim_{N\to\infty} \frac{1}{N\tau} \sum_{i=1}^{N} \ln \left|\frac{d_i}{d_o}\right| . \qquad (21)$$

Here $|d_o|$ is the initial separation in phase space between the original orbit $x_j(t)$ and a neighbouring orbit $x'_j(t)$, $d_o^2 = \Sigma(x_j - x'_j)^2$, where x_j are the ten variables $a_1, \ldots, \alpha$. Both orbits are followed for a short time τ and the final separation $|d_1|$ is recorded. Now the orbit separation is set back to the original value $|d_o|$, but the orientation is chosen at random. Thus after N repetitions or a total time $T = N\tau$, N values of $|d_i|$ are obtained and the expression σ is formed. It can be proved that under suitable conditions σ becomes independent of $|d_o|$ and τ. σ is well suited to illustrating the characteristic difference between regular and chaotic orbits, but is difficult to evaluate for weakly turbulent solutions and hence is no good monitor of the transition region.

IV. CLASSIFICATION OF SOLUTIONS , BIFURCATION DIAGRAM

In this section we present an overview of the possible types of solutions depending on the parameters γ_1 and κ. The results are summarized in the bifurcation diagram shown in Fig. 1. Solving the stationary equations, we find steady-state solutions for practically all points in the γ_1, κ space considered except in a narrow strip along the right-hand boundary, where no bounded solutions exist. But only in the region indicated in Fig. 1 are these solutions stable, with all eigenvalues having negative real parts. On crossing

the boundary of this region there is a Hopf bifurcation characterized by a pair of complex conjugate eigenvalues crossing the imaginary axis. In the adjacent region one finds periodic solutions or limit cycles determined by a single frequency ω_1 (and its harmonics). In the Poincaré map the orbits converge to a finite set of points as the solutions become stationary.

The region where stable periodic orbits exist is bounded by lines where there is a second Hopf bifurcation determined by the appearance of a second frequency. Beyond these lines solutions are in general doubly periodic, orbits covering two - tori in phase space. They are characterized by two generally incommensurable frequencies ω_1, ω_2 (and their combination frequencies). The Poincaré maps are simply closed orbits where, however, some folding may occur. There are two distinct types of tori corresponding to either $\omega_2^{(1)} \sim 0.02\omega$, or $\omega_2^{(2)} \sim \frac{1}{3}\omega$, which we call torus 1 and torus 2. Typical frequency spectra corresponding to these types of solutions are given in Figs. 2 and 3.

No new bifurcation lines appear. The lines separating the limit cycle domain from the torus domain cross at two points. Hence the regions of stable two-tori are bounded by lines where in addition to the second frequency a third frequency seems to appear, $\omega_2^{(2)}$ in addition to $\omega_2^{(1)}$ for torus 1 type and $\omega_2^{(1)}$ in addition to $\omega_2^{(2)}$ for torus 2 type. These lines are found to give the transition to chaotic orbits or turbulence. No stable three-tori are observed. Frequency spectra consistently show that in conjunction with the third discrete frequency broad-band noise appears, characterizing the onset of stochasticity.

No other types of bifurcations are found, in particular no period-doubling bifurcations. In fact, the behaviour displayed in Fig. 1 corresponds precisely to the Ruelle-Takens picture of the

transition to turbulence and is in contrast to the transition via a sequence of period-doubling bifurcations, the Feigenbaum model, which is realized in several three-dimensional dynamical systems such as the three-wave mode-coupling equations by Wersinger et al.[12]. It is interesting to compare their results with those presented here. While in Ref. 12 the increase of complexity (period doubling) and transition to turbulence occurs when increasing the wave damping, in our case chaos occurs when the driving of the unstable mode is increased, while no chaotic orbits are found in the case of weak driving, $\gamma_1 \to 0$. Although parameters are in general different, in particular the ratio $|\gamma_t|/\Delta\omega$, which is larger in Ref. 12 (stronger damping) than in our case, the origin of the different types of behaviour observed seems to stem from the higher dimensionality of the present model. It is well-known that because of phase space contraction along the orbit two-tori do not exist in three-dimensional systems. On the other hand, higher-dimensional approximations of the Rayleigh-Bénard equations such as the 14-dimensional truncation recently studied by Curry[14] or the N-dimensional truncations, $N \leqq 136$ by Maschke et al.[15] show a similar sequence of two Hopf bifurcations as in our case in contrast to the three-dimensional Lorenz model.

V. DISCUSSION OF PARTICULAR TRANSITIONS

In this section we discuss in greater detail the behaviour along two specific paths in γ_1, κ space as well as the transition to vanishing κ corresponding to the model of Terry and Horton[7], these being indicated by short, heavy lines in Fig. 1. We first consider the change of the solution as γ_1 is increased for constant $\kappa = 0.65$. The first Hopf bifurcation from steady state to a periodic solution with $\omega_1 \cong 2.0$ occurs at $\gamma_1 \cong 0.119$, the second Hopf bifurca-

tion to a two-torus with $\omega_2 = \omega_2^{(1)} \cong .03$ at $\gamma_1 \cong 0.121$, while the third frequency $\omega_3 = \omega_2^{(2)} \cong 0.6$ appears at $\gamma_1 \cong 0.1375$, which marks the onset of turbulence. Frequency spectra illustrating the different states are shown in Fig. 4a - d. It is interesting to note that the contribution of the second (low) frequency $\omega_2^{(1)}$ is strongest close to the lower bifurcation point $\gamma_1 \cong 0.121$, leading to a strongly modulated oscillation as shown in Fig. 5 (at t = 2000 the solution has nearly reached its asymptotic state). When γ_1 is increased, the $\omega_2^{(1)}$ line becomes weaker and almost vanishes near the upper bifurcation point $\gamma_1 \cong 0.1375$. For $0.136 \lesssim \gamma_1 \lesssim 0.1375$ the solution is again almost simply periodic with maximum amplitude, $a_{1\min} \cong 0$. At the bifurcation point $\omega_2^{(1)}$ reappears together with the third frequency $\omega_2^{(2)}$. Along with the discrete frequencies broad-band noise is generated, Fig. 4c, which for larger values of γ_1 completely dominates the spectrum, Fig. 4 d. The Poincaré maps of a_2 vs. a_1 and a_3 vs. a_1 for the doubly periodic case $\gamma_1 = 0.13$ are given in Fig. 6. Note the folding of the projected orbit which occurs when a_j come close to zero. Other combinations such as b_2 vs b_1 show similar maps as is expected if the orbit covers a two-torus.

The second path in γ_1, κ space, which we follow in detail, is the vertical line $\gamma_1 = 0.09$ for $0.3 \gtrsim \kappa \gtrsim 0.2$. Decreasing κ we encounter a bifurcation at $\kappa = 0.267$, where in addition to the frequency ω_1 a second frequency $\omega_2 = \omega_2^{(2)}$ appears, Fig. 7a. Between this value and $\kappa = .225$ the motion is in general doubly periodic, i.e. the orbit covers a two-torus in phase space. There is, however, a strong tendency to locking of the frequency ratio to certain rational numbers, which makes the solution almost or exactly periodic. This behaviour is shown in Fig. 8, while Fig. 7b and c give the frequency spectra for $\kappa = 0.264$ where $\omega_1/\omega_2 = 7/2$, and for $\kappa = 0.243$ where $\omega_1/\omega_2 = 18/5$. The range of frequency ratio locking terminates at $\kappa = .225$, where the solution becomes turbulent, probably owing to the appearance of a third low frequency component, Fig. 7 d. The

transition to a visibly turbulent solution is very sharp in this case. It should be noted that there is no region of hysteresis, the transition occurring at the same point whether moving downward or upward in κ.

Let us now consider the transition $\kappa \to 0$. Since it occurs at rather small values of κ it could not have been resolved on the global bifurcation diagram in Fig. 1. For the present choice of parameters the Terry - Horton equations do not give rise to stochastic solutions. There is a periodic solution for $0 \leqq \gamma_1 \lesssim 0.12$ and a steady-state solution for $0.12 \lesssim \gamma_1 \leqq .2475$, while for $\gamma_1 > .2475$ no bounded solutions exist. The sequence shown in Fig. 9 illustrates the transition $\kappa \to 0$ for $\gamma_1 = 0.09$. For $\kappa = 0.025$ the solution is still strongly turbulent, Fig. 9a; for $\kappa = 0.008$, Fig. 9b, it is weakly turbulent, but with the main frequency being significantly different from the lines characterizing the periodic solution at $\kappa = 0$. The latter solution only becomes apparent for $\kappa < 0.003$, see Fig. 9c for $\kappa = 0.0016$. Hence we find that at least for the present set of parameters the Terry - Horton model is quite exceptional, being valid only at very small values of the parallel wavelength, $\kappa << 0.01$.

Finally, in Fig. 10 a, b is plotted the Liapunov exponent as defined in eq. (21) for a regular, doubly periodic solution ($\gamma_1 = 0.122$, $\kappa = 0.65$) and a stochastic state ($\gamma_1 = 0.09$, $\kappa = 0.16$). In both cases one has $N = 500$ and $\tau = 10$. While in the first case σ slowly approaches zero, it remains finite in the second, $\sigma \cong 0.055$.

VI. CONCLUSIONS

We have investigated the interaction of three sound-drift-waves, an obvious extension of the three-drift-wave model of Terry and Horton to include the effect of the coupling of drift waves to sound waves

owing to the presence of finite parallel wavelength (which always arises in a sheared magnetic field). Whereas in a companion paper[10] parameters corresponding to a particular drift instability are considered, our present interest is in the generic properties of this ten-dimensional model, in particular the bifurcation sequence and transition to turbulence. As illustrated in the bifurcation diagram in Fig. 1, there are only four possible states: steady-state solutions, periodic, doubly periodic and turbulent orbits. No regular states with more than two independent frequencies seem to exist. The appearance of a third discrete frequency is intimately linked to the existence of broad-band noise, which is the very definition of turbulence. Hence the model gives a nearly perfect example of the Ruelle-Takens[16] route to turbulence:

steady state (fix point)

→ Hopf bif. periodic orbit (limit cycle)

→ Hopf bif. doubly periodic orbit (2-torus)

→ (Hopf bif.) turbulence (= unstable 3-torus ?)

This is in contrast to the period doubling route (including tangent bifurcations) of Feigenbaum, which is realized in most low-dimensional (particularly three-dimensional) systems. No period doubling bifurcation at all is found in our model, though its existence for other values of the parameters cannot be completely excluded. No case of hysteresis, i.e. dependence of the asymptotic solution on the initial conditions, was observed, nor any strongly intermittent turbulent solutions. The case $\kappa = 0$ appears to be rather exceptional, at least for the present choice of parameters.

Solutions are quite different (and nonturbulent) from those at finite $\kappa \cong 0.1 - 1$, the transition taking place at small κ - values, $\kappa < 0.01$.

ACKNOWLEDGEMENTS

One of the authors (H.K.) would like to thank A. Salat for useful discussions and R. Meyer-Spasche and H. Welter for their help with the numerical calculation.
This work was performed under the terms of the agreement on association between Max-Planck-Institut für Plasmaphysik and EURATOM.

REFERENCES

1) E. Mazzucato, Phys. Rev. Lett 48, 1828 (1982)

2) C.M. Surko and R.E. Slusher, Phys. Fluids 23, 2425 (1980)

3) S.P. Hirschman and K. Molvig, Phys. Rev. Lett. 42, 648 (1979)

4) C.W. Horton, Phys. Rev. Lett. 37, 1269 (1976)

5) A. Hasegawa and K. Mima, Phys. Fluids 21, 87 (1978)

6) E.N. Lorenz, J. Atmos. Sci 20, 130 (1963)

7) P.W. Terry and C.W. Horton, Phys. Fluids 25, 491 (1982)

8) P.W. Terry and C.W. Horton, Phys. Fluids 26, 106 (1983)

9) R.E. Waltz, Phys. Fluids 26, 169 (1983)

10) He Kaifen and D. Biskamp, submitted to Phys. Lett. A

11) D. Biskamp and M. Walter, 1984 Sherwood Theory Conference, Incline Village, paper 2R5

12) J.M. Wersinger, J.M. Finn, and E. Ott, Phys. Fluids 23, 1142 (1980)

13) G. Benettin, L. Galgani, and J.M. Strelcyn, Phys. Rev. A 14, 2338(1976)

14) J.H. Curry, Commun. Math. Phys. 60, 193 (1978)

15) E.K. Maschke and B. Saramito, Physica Scripta T2/2, 410 (1982)

16) D. Ruelle and F. Takens, Commun. Math. Phys. 20, 167 (1971)

FIGURE CAPTIONS

Fig. 1 $\gamma_1 - \kappa$ bifurcation diagram.

Fig. 2 Frequency spectrum of a typical torus 1 type solution.

Fig. 3 Frequency spectrum of a typical torus 2 type solution.

Fig. 4 Frequency spectra of orbits encountered along the path $\kappa = 0.65$:
a) periodic orbit; b) doubly periodic orbit;
c) simultaneous appearance of third frequency and broad-band noise; d) strongly turbulent state.

Fig. 5 Time trace of $a_1(t)$ corresponding to the parameters of case b) in Fig. 4.

Fig. 6 Poincaré plots of a_2, a_3 vs. a_1 for two different cross-sections: $\alpha = \pi/2$ and $3\pi/2$.

Fig. 7 Frequency spectra of orbits encountered along the path $\gamma_1 = 0.09$
a) doubly periodic orbit; b) periodic orbit with $\omega_1/\omega_2 = 7/2$ and basic frequency $\omega_e \cong 0.15$; c) periodic orbit with $\omega_1/\omega_2 = 18/5$ and $\omega_e \cong 0.06$; d) appearance of ω_3 and onset of turbulence.

Fig. 8 Frequency ratio ω_1/ω_2 in the κ - range of existence of torus solution for $\gamma_1 = 0.09$.

Fig. 9 Frequency spectra illustrating the transition $\kappa \to 0$ for $\gamma_1 = 0.09$.

Fig. 10 Maximum Liapunov exponent σ for a) regular orbit (torus) b) turbulent state.

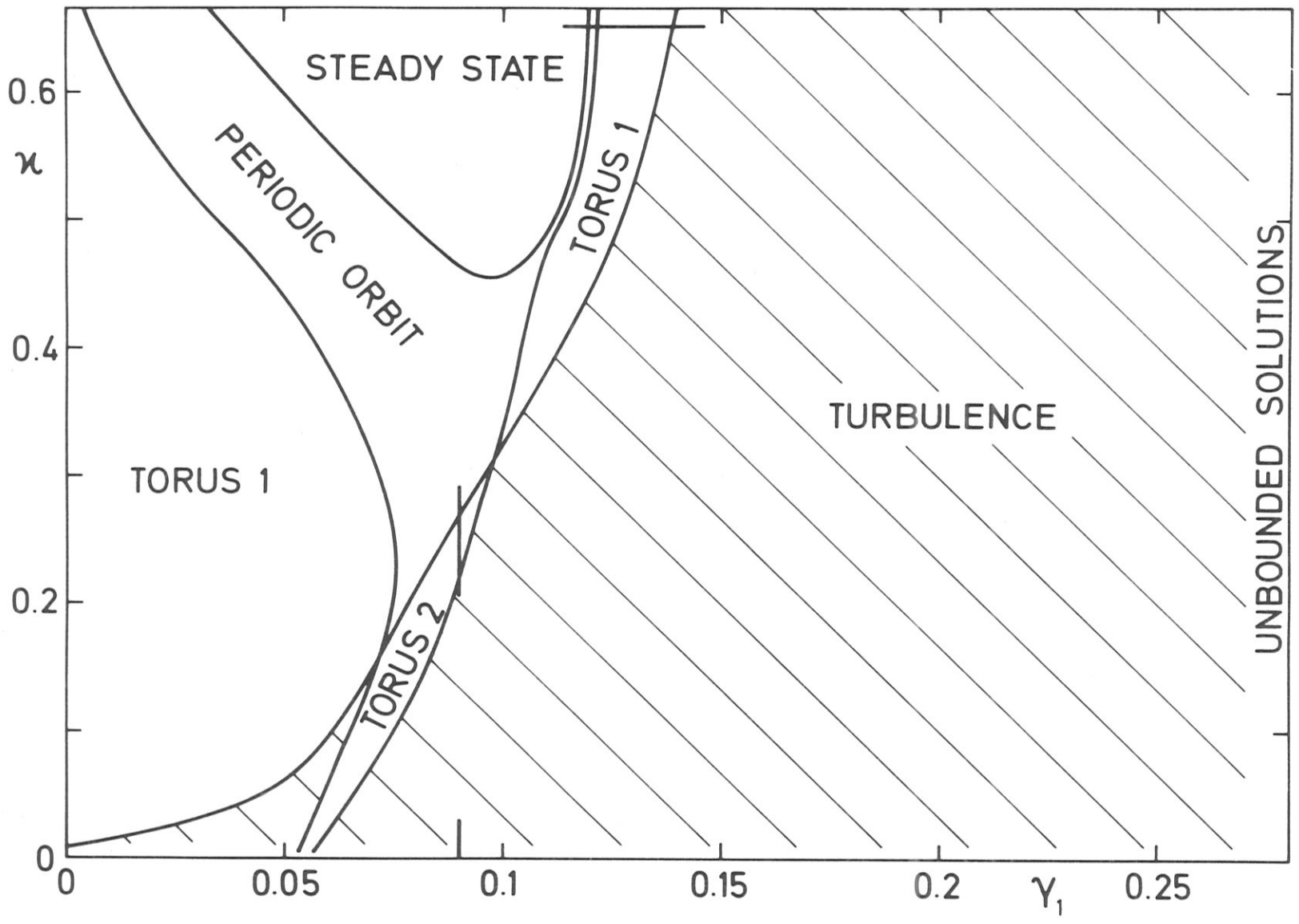
STEADY STATE
PERIODIC ORBIT
TORUS 1
TORUS 1
TORUS 2
TURBULENCE
UNBOUNDED SOLUTIONS
0.6
0.4
0.2
0
0
0.05
0.1
0.15
0.2
0.25
γ_1

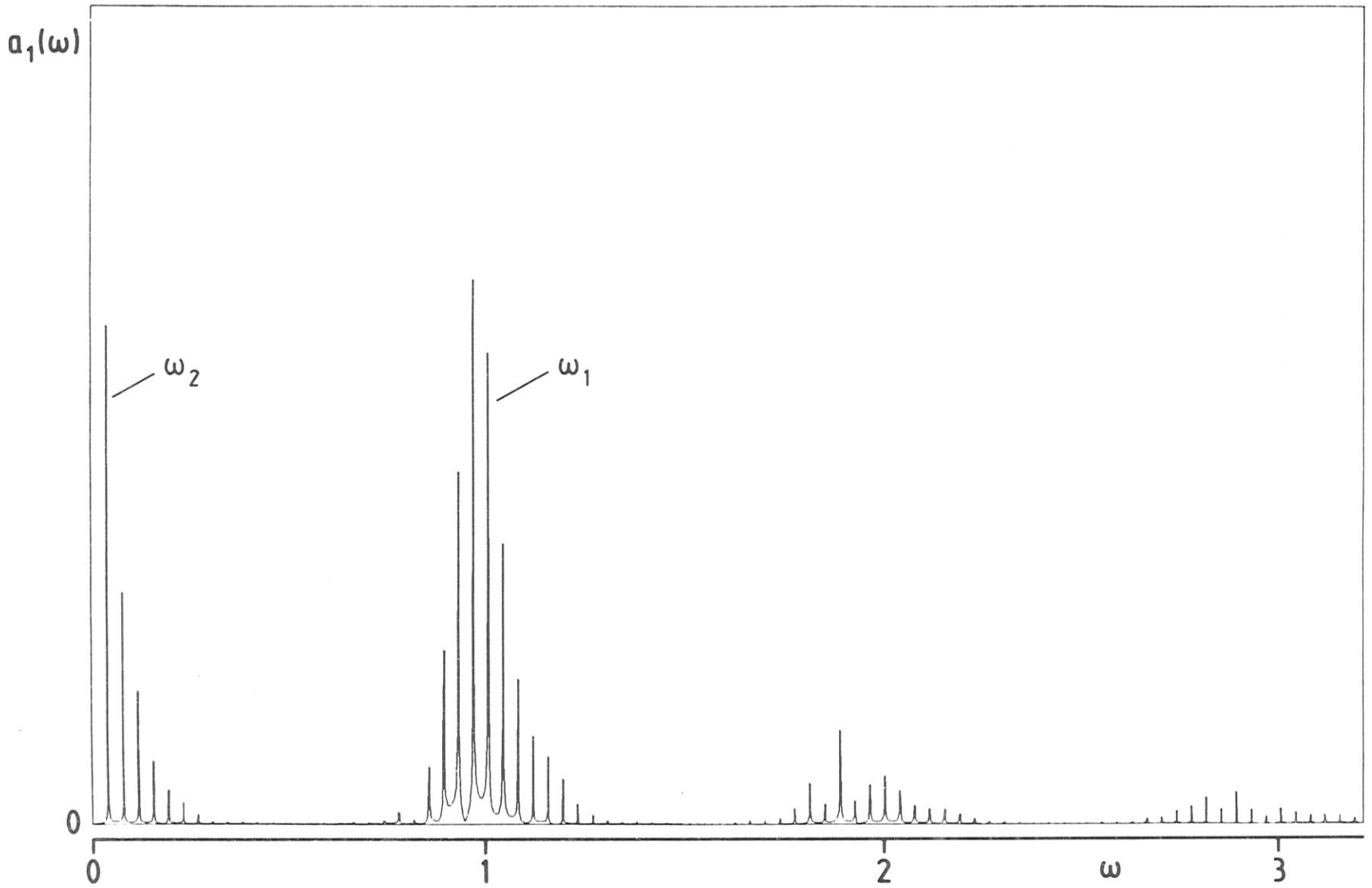
$a_1(\omega)$
ω_2
ω_1
0
0
1
2
ω
3

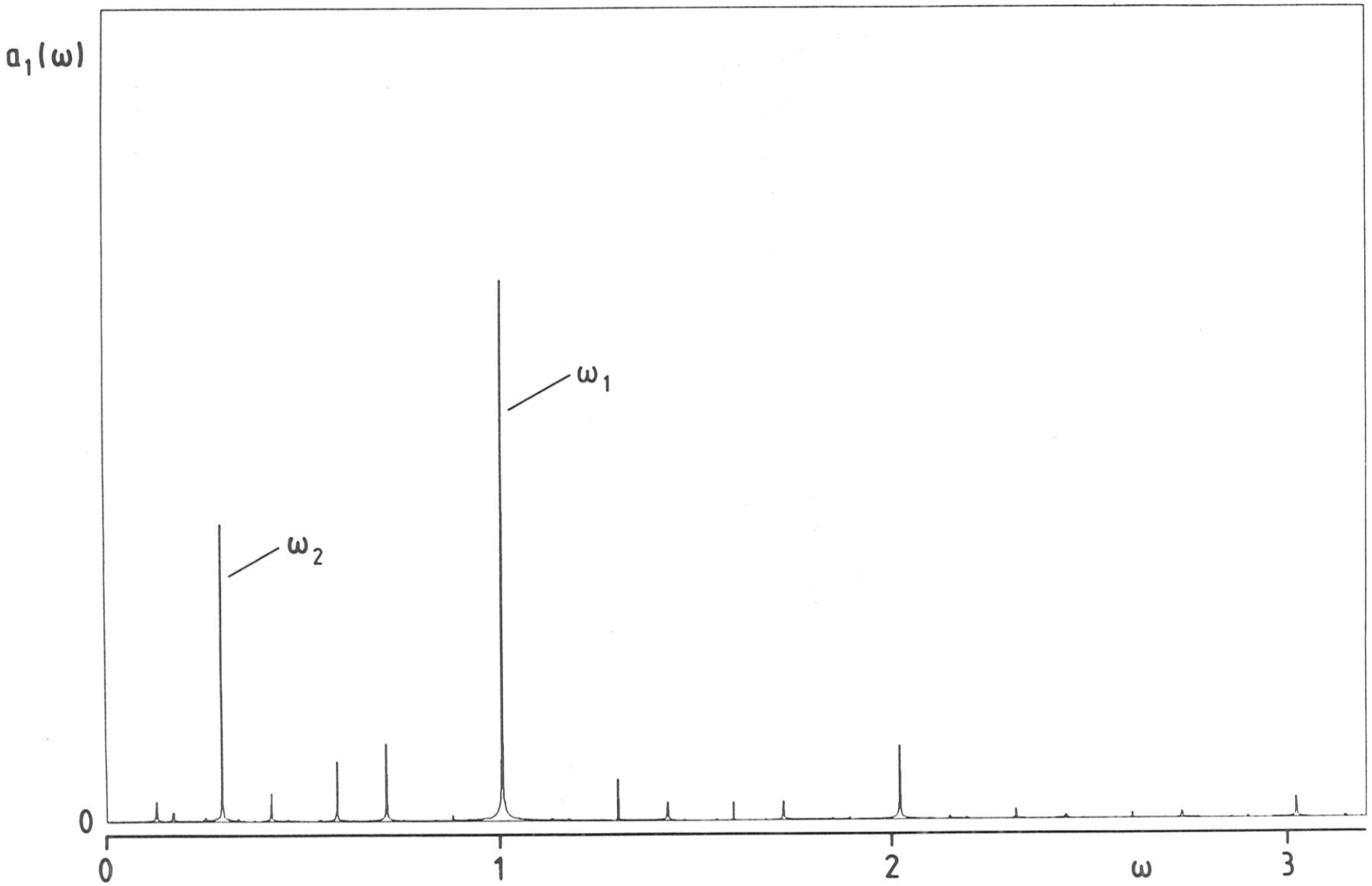
$a_1(\omega)$
ω_1
ω_2
0
0
1
2
ω
3

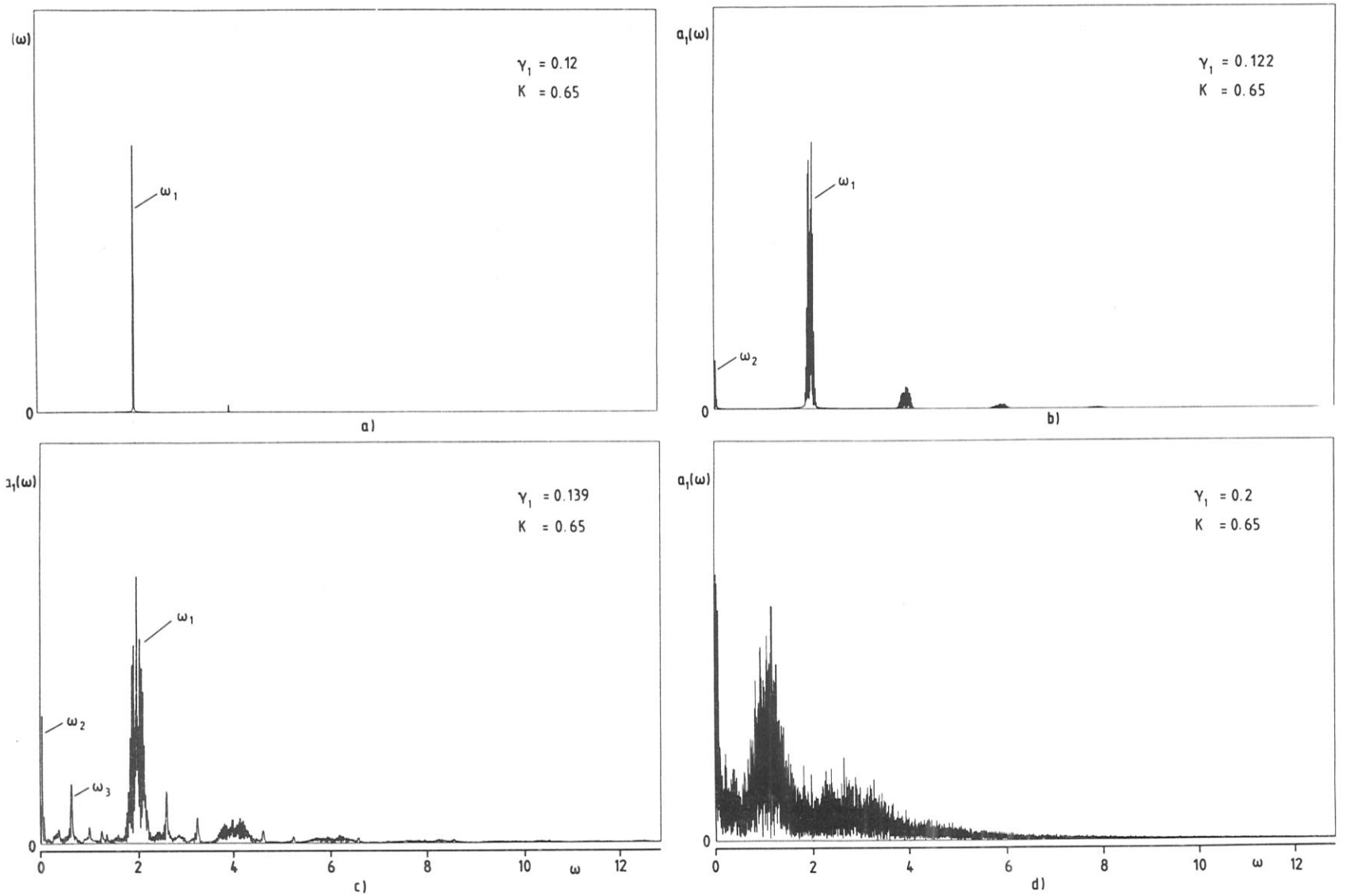
(ω)
γ1 = 0.12
K = 0.65
ω1
0
a)
a1(ω)
γ1 = 0.122
K = 0.65
ω1
ω2
0
b)
a1(ω)
γ1 = 0.139
K = 0.65
ω1
ω2
ω3
0
0 2 4 6 8 10 ω 12
c)
a1(ω)
γ1 = 0.2
K = 0.65
0
0 2 4 6 8 10 ω 12
d)

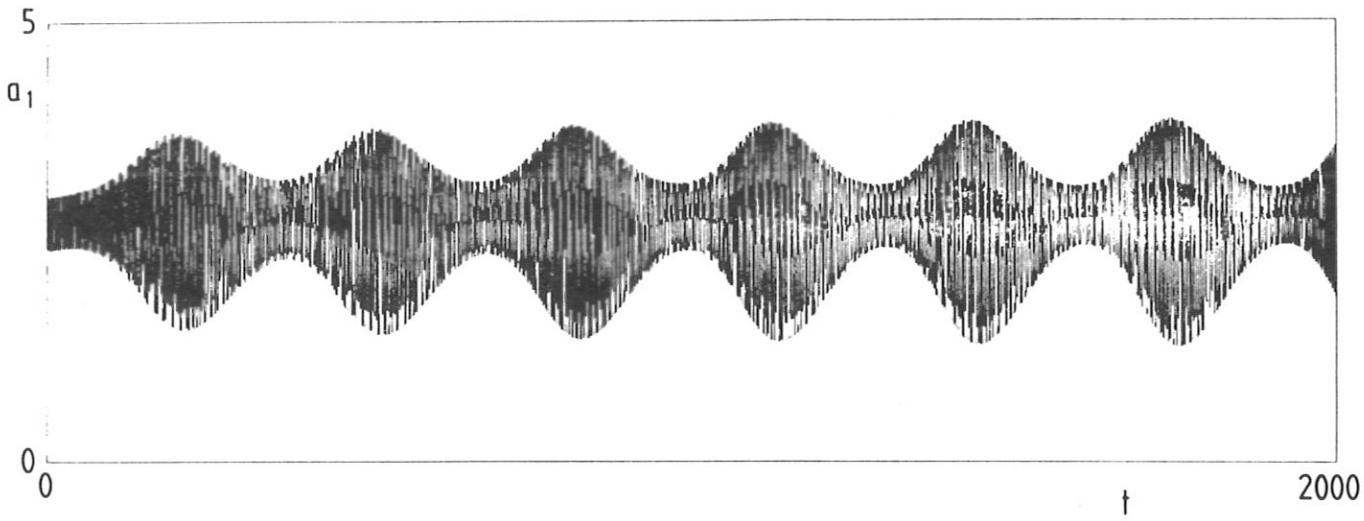
5
a_1
0
0
t
2000

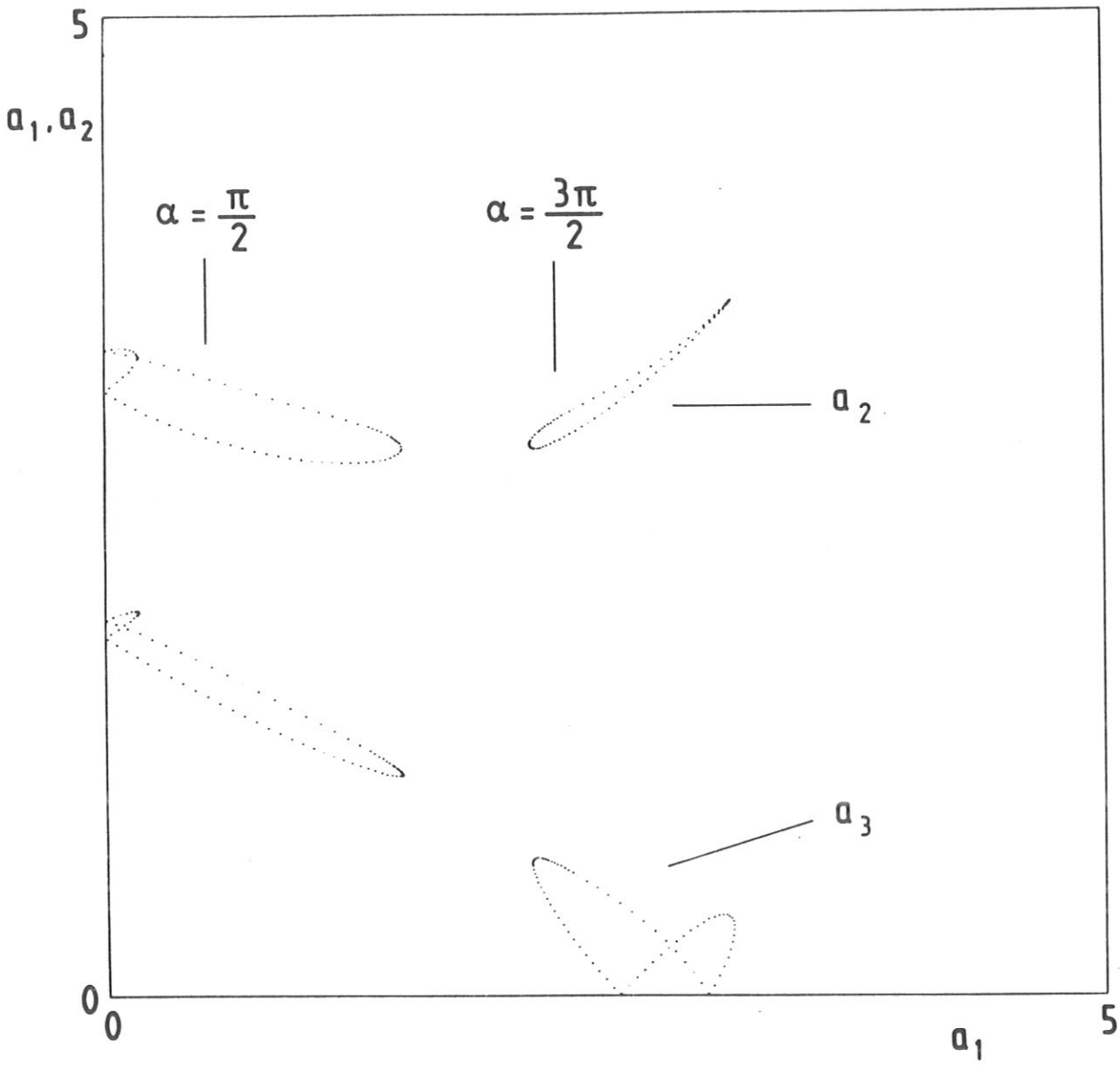
5
a_1, a_2
$\alpha = \frac{\pi}{2}$
$\alpha = \frac{3\pi}{2}$
a_2
a_3
0
0
a_1
5

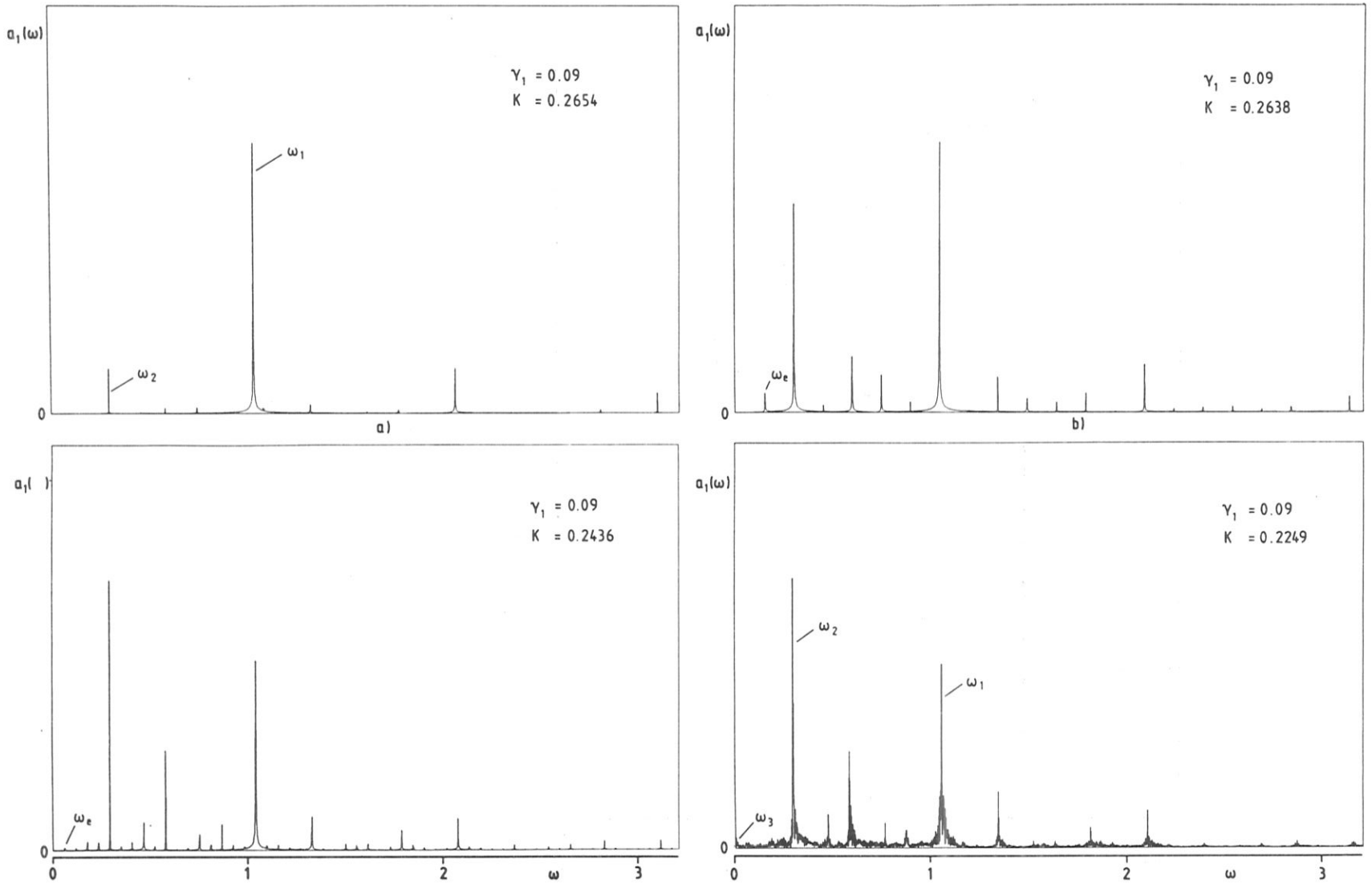
$a_1(\omega)$
$\gamma_1 = 0.09$
$K = 0.2654$
ω_1
ω_2
0
a)
$a_1(\omega)$
$\gamma_1 = 0.09$
$K = 0.2638$
ω_e
0
b)
$a_1($
$\gamma_1 = 0.09$
$K = 0.2436$
ω_e
0
0
1
2
ω
3
$a_1(\omega)$
$\gamma_1 = 0.09$
$K = 0.2249$
ω_2
ω_1
ω_3
0
0
1
2
ω
3

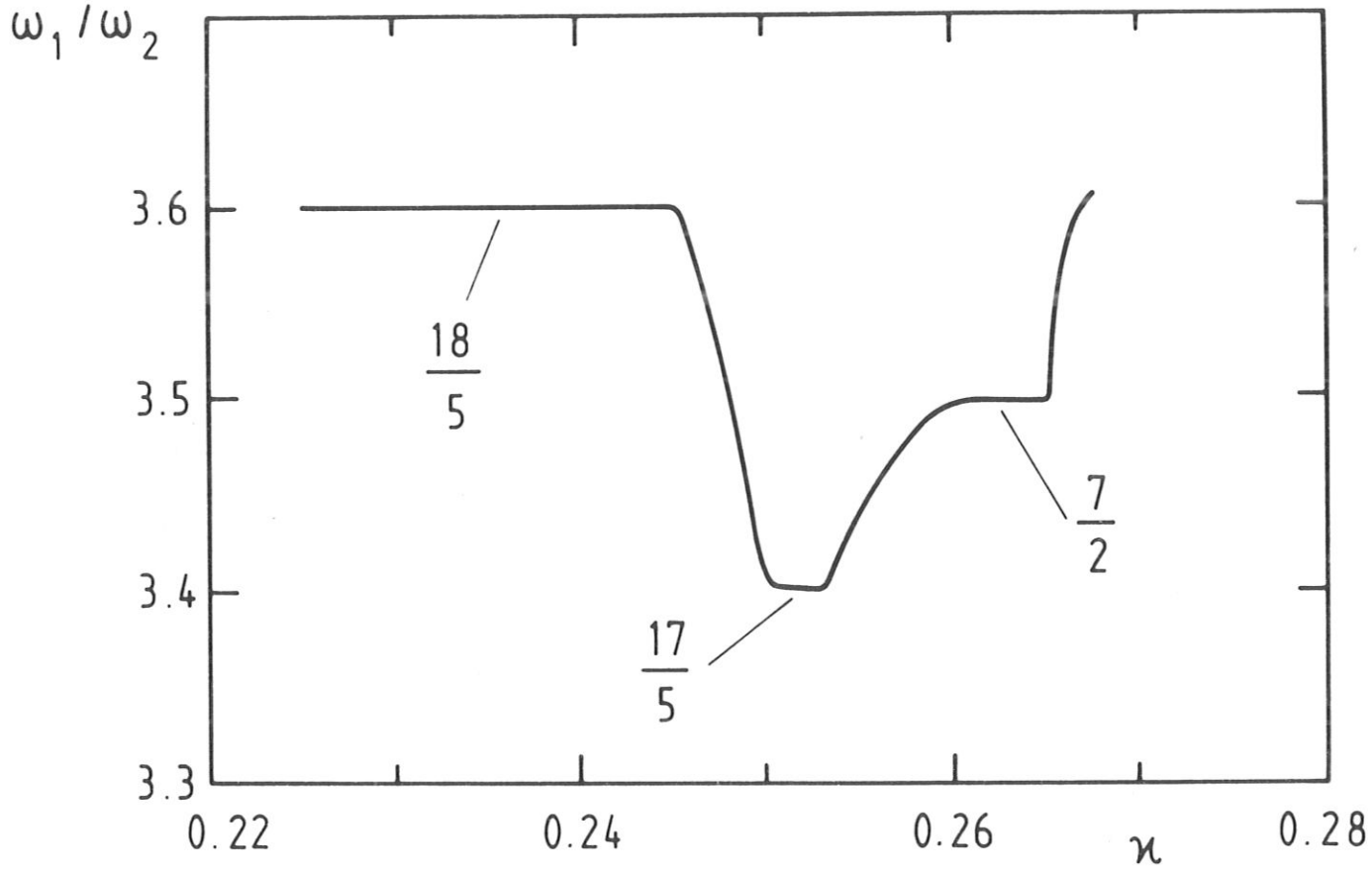
ω_1/ω_2
3.6
3.5
3.4
3.3
0.22
0.24
0.26
0.28
$\varkappa$
$\frac{18}{5}$
$\frac{17}{5}$
$\frac{7}{2}$

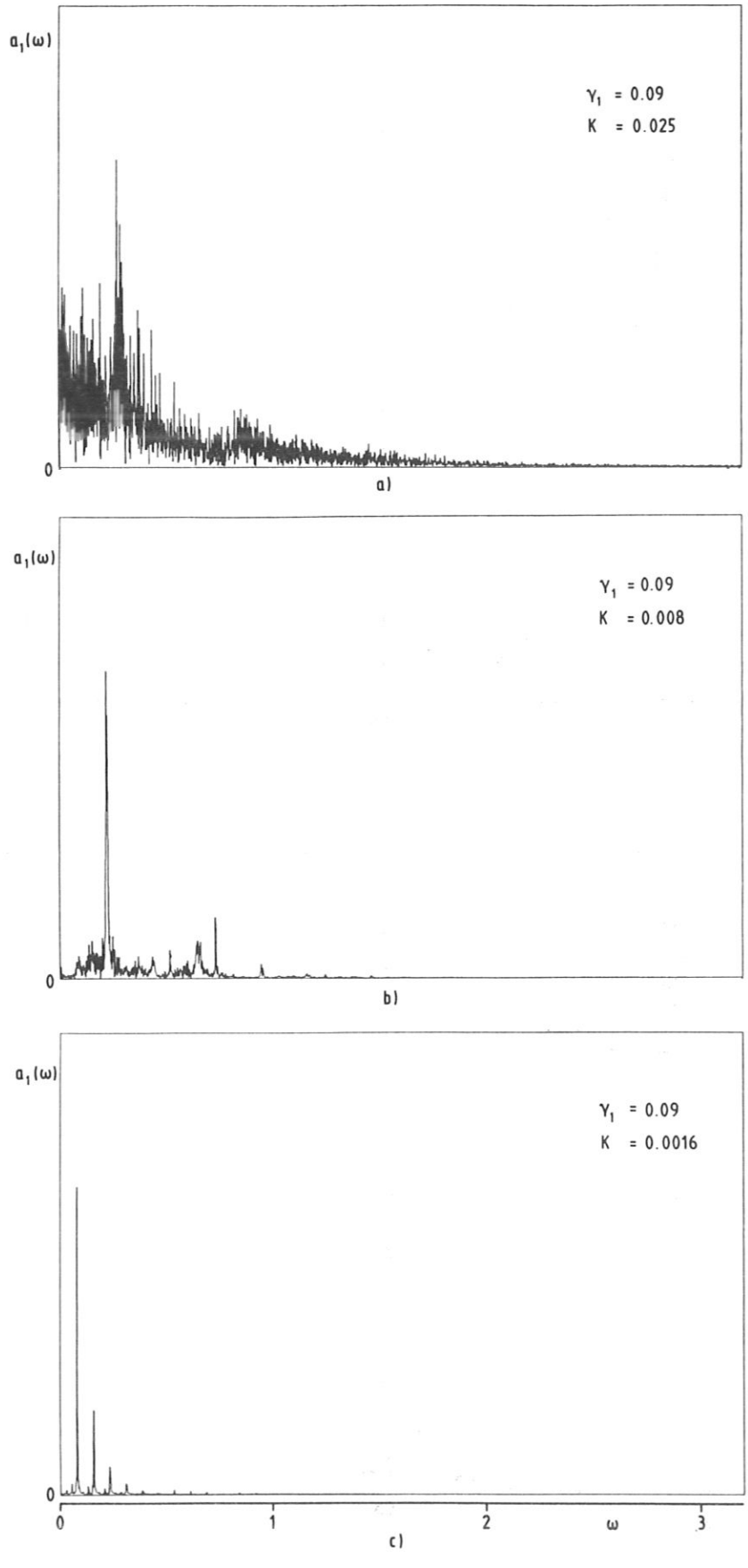
$a_1(\omega)$
$\gamma_1 = 0.09$
$K = 0.025$
0
a)
$a_1(\omega)$
$\gamma_1 = 0.09$
$K = 0.008$
0
b)
$a_1(\omega)$
$\gamma_1 = 0.09$
$K = 0.0016$
0
0
1
2
ω
3
c)

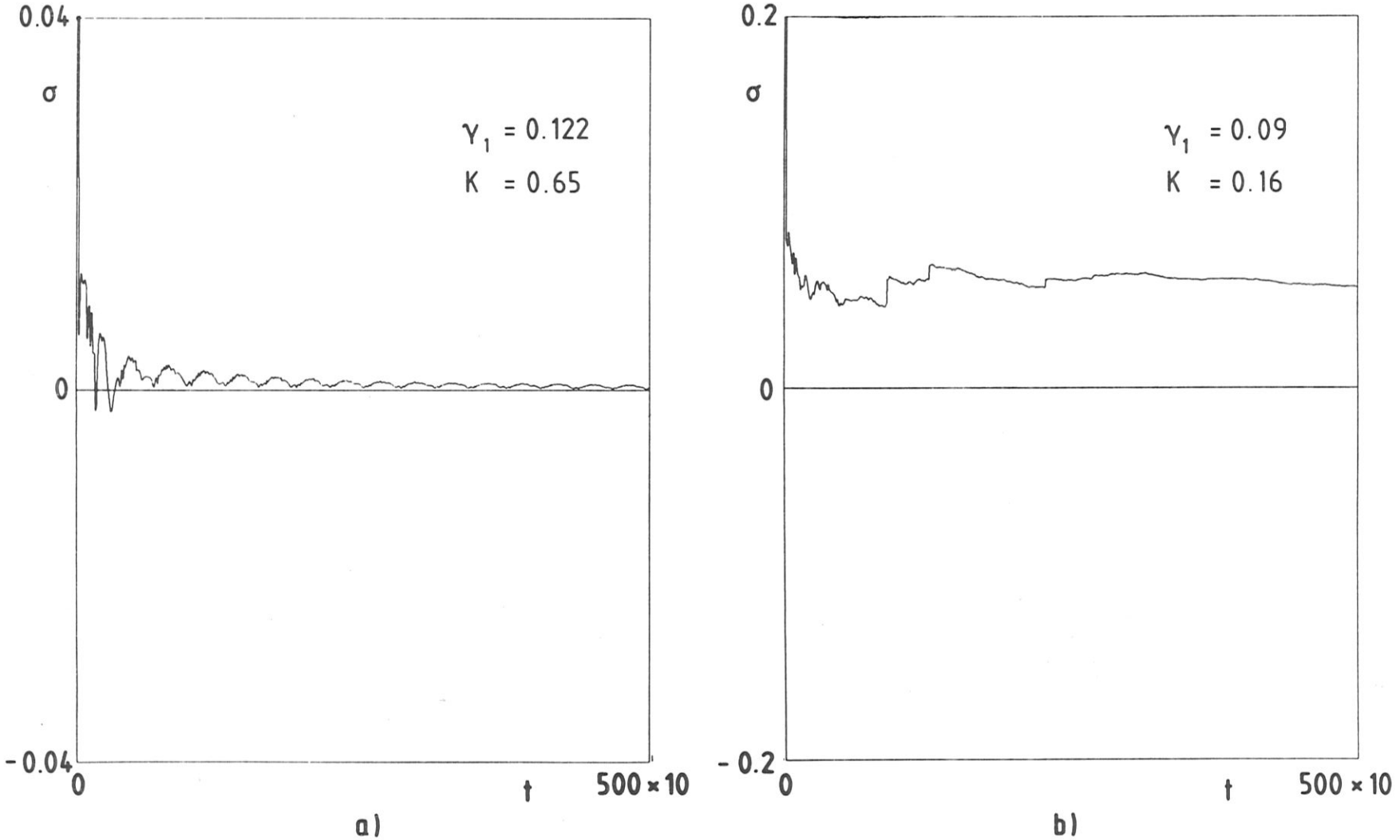
0.04
σ
γ_1 = 0.122
K = 0.65
0
-0.04
0
t
500 × 10
a)
0.2
σ
γ_1 = 0.09
K = 0.16
0
-0.2
0
t
500 × 10
b)